iScience, Volume *26*

Supplemental information

Molecular basis for antiviral activity of two pediatric neutralizing antibodies targeting SARS-CoV-2 Spike RBD

Yaozong Chen, Jérémie Prévost, Irfan Ullah, Hugo Romero, Veronique Lisi, William D. Tolbert, Jonathan R. Grover, Shilei Ding, Shang Yu Gong, Guillaume Beaudoin-Bussières, Romain Gasser, Mehdi Benlarbi, Dani Vézina, Sai Priya Anand, Debashree Chatterjee, Guillaume Goyette, Michael W. Grunst, Ziwei Yang, Yuxia Bo, Fei Zhou, Kathie Béland, Xiaoyun Bai, Allison R. Zeher, Rick K. Huang, Dung N. Nguyen, Rebekah Sherburn, Di Wu, Grzegorz Piszczek, Bastien Paré, Doreen Matthies, Di Xia, Jonathan Richard, Priti Kumar, Walther Mothes, Marceline Côté, Pradeep D. Uchil, Vincent-Philippe Lavallée, Martin A. Smith, Marzena Pazgier, Elie Haddad, and Andrés Finzi

Table S1. Summary of biolayer interferometry kinetic constants. Related to Table 1 and Figure S2C.

Analyte	Immobilized ligand	Fitting mode	k_a ($M^{-1}s^{-1}$)	k_d (s^{-1})	K_D (pM)	K_D reduction fold compared to RBD_{WT}
EH3 IgG	RBD_{WT}	1:1	1.01×10^5	6.09×10^{-7}	6.06	1
	RBD_{E484K}	1:1	1.11×10^5	4.46×10^{-7}	4.04	0.67
EH8 IgG	RBD_{WT}	1:1	2.11×10^5	3.55×10^{-7}	1.68	1
	RBD_{E484K}	1:1	1.83×10^5	6.01×10^{-7}	3.29	1.96

Table S2. Data collection and model refinement statistics. Related to Figure 3.

	EH3-RBD	EH8-RBD
Data collection		
Wavelength, Å	0.979	0.979
Resolution range, Å	34.38 - 2.65 (2.745 - 2.65)	46.91 - 2.49 (2.58 - 2.49)
Space group	$P\ 2_1\ 2\ 2_1$	$P\ 2_1\ 2\ 2_1$
Unit cell parameter		
a, b, c, Å	86.7, 103.1, 112.3	81.8, 100.7, 106.0
α, β, γ, °	90.0, 90.0, 90.0	90.0, 90.0, 90.0
Redundancy	6.6	18.8
Completeness, %	99.21 (98.85)	99.20 (92.82)
Mean I/sigma(I)	10.37 (2.28)	30.40 (2.67)
R_{merge}[a]	0.190 (0.720)	0.144 (1.037)
R_{pim}[b]	0.079 (0.301)	0.034 (0.259)
$CC_{1/2}$[c]	0.933 (0.772)	0.996 (0.877)
Wilson B_{factor}, (1/Å^2)[d]	39.62	57.01
Refinement		
R_{work}[e]	0.179 (0.245)	0.244 (0.425)
R_{free}[f]	0.221 (0.305)	0.270 (0.431)
Resolution, Å	34.38 - 2.65	46.91 - 2.49
# of non-hydrogen atoms		
proteins	4968	4829
ligands		
water	144	102
Overall B_{factor}, (Å^2)		
proteins	45.13	62.54
ligands	99.79	96.86
water	42.48	49.96
RMS (bond lengths), Å	0.004	0.005
RMS (bond angles), °	0.74	0.89
Ramachandran[g]		
Favored, %	97.11	96.96
Allowed, %	2.73	3.04
Outliers, %	0.16	0.00
PDB ID	7UL1	7UL0

Statistics for the highest-resolution shell are shown in parentheses.

[a] $R_{merge} = \sum |I - \langle I \rangle| / \sum I$, where I is the observed intensity and $\langle I \rangle$ is the average intensity obtained from multiple observations of symmetry-related reflections after rejections

[b] R_{pim} = as defined in [45].

[c] $CC_{1/2}$ = as defined by Karplus and Diederichs [46]

[d] Wilson B_{factor} as calculated in [47]

[e] $R = \sum \| F_o| - |F_c\| / \sum |F_o|$, where F_o and F_c are the observed and calculated structure factors, respectively.

[f] R_{free} = as defined by Brünger [48]

[g] Calculated with MolProbity [49].

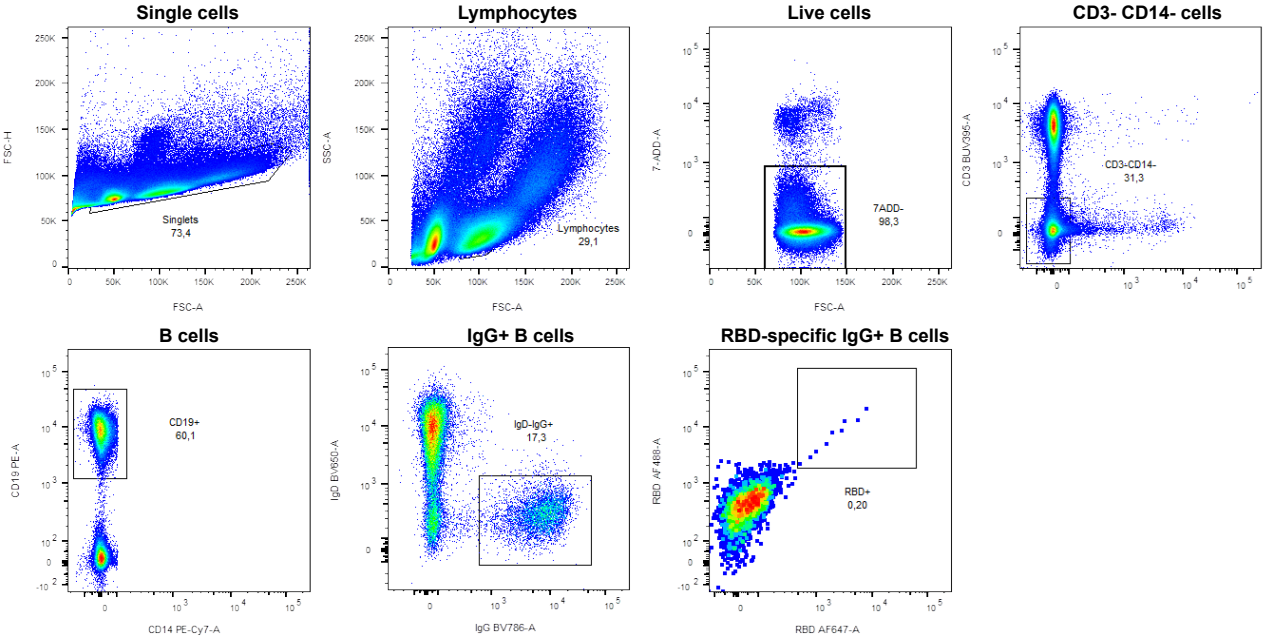

Figure S1. Gating strategy for the isolation of RBD-specific mAbs. Related to Figure 1.
Flow cytometry gates to identify RBD-specific B cells from PBMCs of a pediatric patient (Patient 12). RBD-specific B cells were identified according to cell morphology by light-scatter parameters and excluding doublets cells while gating on live cells (7-AAD-). Cells were then gated based on lineage markers: CD3- (T cell marker), CD14- (monocyte marker) and CD19+ (B cell marker). Cells were further gated for isotypic expression: IgD- (naïve) and IgG+ (class-switched). Finally, RBD-specific IgG+ B cells were identified using a dual staining with fluorescent RBD probes (RBD-AF647 and RBD-AF488). The nine RBD-specific B cells were sorted as single cells to clone their BCR sequence.

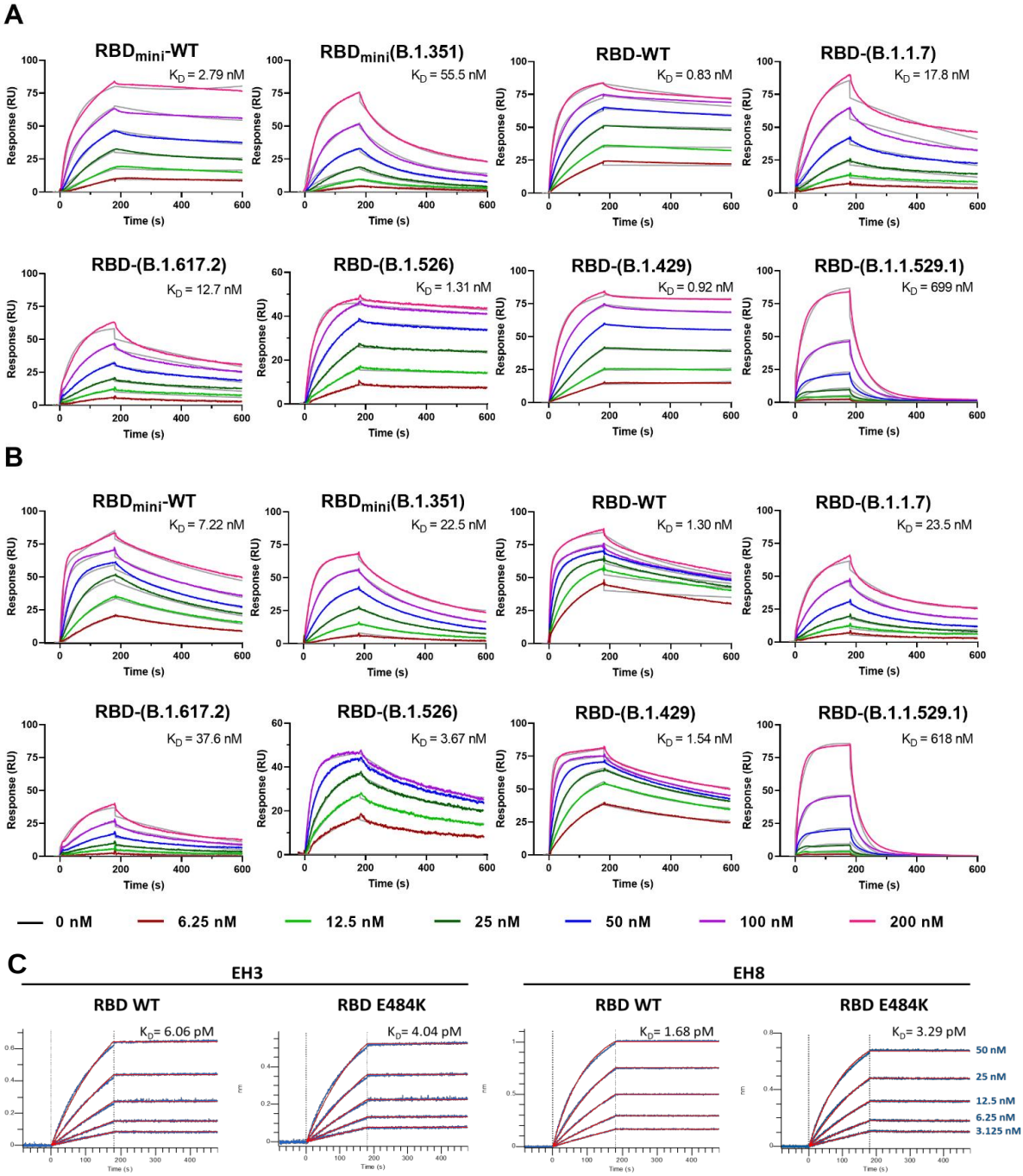

Figure S2. Binding affinity of RBDs of SARS-CoV-2 VOCs to EH3 and EH8. Related to Table 1.
(**A-B**) SPR kinetic measurement of SARS-CoV-2 RBDs binding to immobilized (**A**) EH3 IgG and (**B**) EH8 IgG. Either IgGs (~250-350 RU) were immobilized on a Protein A chip and 2-fold dilutions of SARS-CoV-2 RBDs of WT and 6 VOCs (6.25-200nM) were injected as flow analytes. The experimental sensorgrams are colored in indicated colors and the 1:1 Langmuir fitting are in grey. RBD_{mini} is the segment of residue 329-527 and otherwise are residue 319-537. The detailed SPR kinetic constants are listed in **Table 1**. (**C**) Binding kinetics between SARS-CoV-2 RBD (WT or E484K) and EH3 or EH8 mAbs assessed by biolayer interferometry. Biosensors loaded with RBD proteins were soaked in two-fold dilution series of indicated mAbs (50 nM**–**3.125 nM) at 25°C. Raw data are shown in blue and 1:1 binding model is shown in red. The detailed biolayer interferometry kinetic constants are listed in **Table S1**.

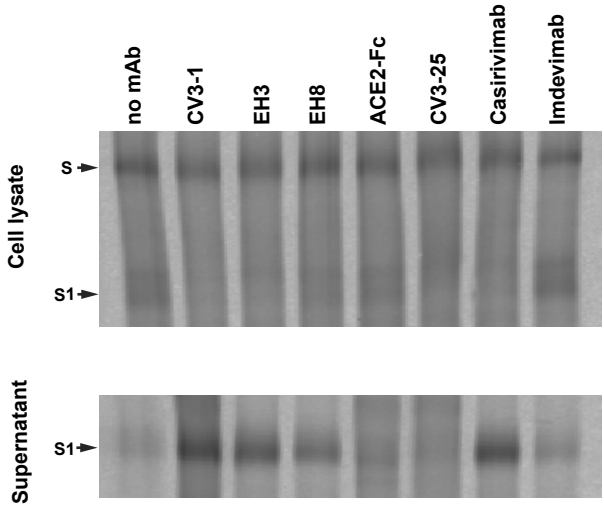

Figure S3. The ability of RBD-specific mAbs to induce S1 shedding is epitope-dependent. Related to Figure 4.

S1 shedding was evaluated by transfection of 293T cells to express SARS-CoV-2 S D614G followed by radiolabeling using 35S-methionine/cysteine mix in presence of RBD-specific mAbs (CV3-1, EH3, EH8), ACE2-Fc, S2-specific CV3-25, or two FDA-approved RBD-specific mAbs (Casirivimab and Imdevimab). This was followed by immunoprecipitation of cell lysates and supernatant with CV3-25 and a rabbit antiserum raised against SARS-CoV-2 RBD produced in-house. Samples were analyzed by SDS-PAGE and autoradiography.

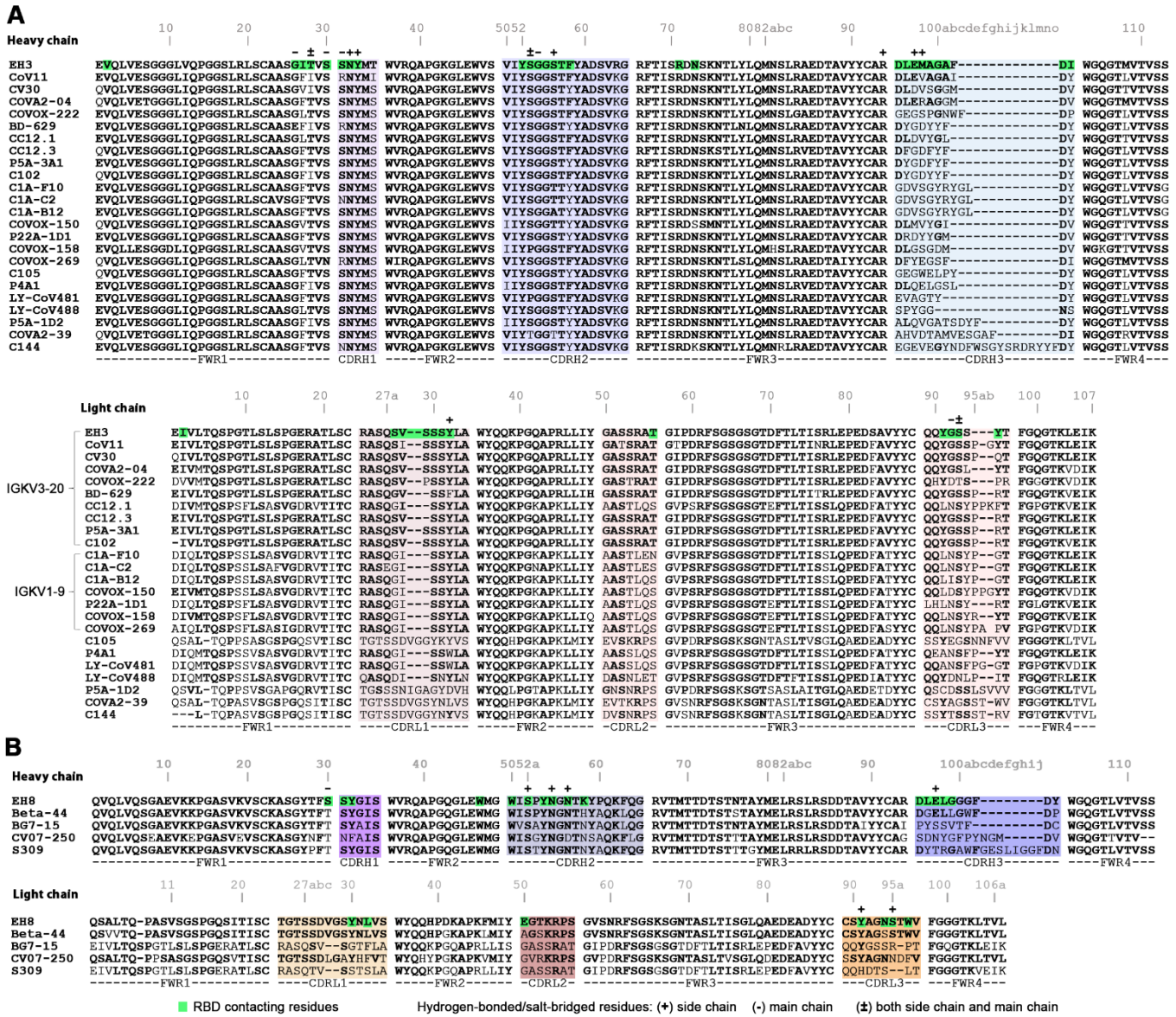

Figure S4. V_H and V_L sequence alignments of EH3 and EH8 to other structurally available RBD-specific mAbs. Related to Figure 4.

(**A**) Alignments of EH3 and other 23 IGHV3-53 encoded Abs. (**B**) Alignments of EH8 and other 4 IGHV1-18 Abs. The RBD-contacting residues (BSA>0) in EH3-RBD and EH8-RBD crystal structures are shaded in green. Residues involved in salt-bridges or H-bonds to the RBD are marked above the sequence with (+) for the side chain, (-) for the main chain and (±) for both.